Acta Crystallographica Section D
Biological Crystallography
ISSN 0907-4449

Structure of *Haemophilus influenzae* HslU protein in crystals with one-dimensional disorder twinning

Christine B. Trame and David B. McKay*

Department of Structural Biology, Stanford University School of Medicine, Stanford, CA 94305, USA

Correspondence e-mail: dave.mckay@stanford.edu

Received 18 December 2000
Accepted 9 May 2001

PDB References: HslU, 1g41; SeMet-HslU, 1im2.

The structure of the *Haemophilus influenzae* HslU protein, a molecular chaperone of the Clp/Hsp100 family, has been solved to 2.3 Å by molecular replacement using a model of the homologous *Escherichia coli* protein. The crystals in which the structure was solved have an unusual twinning, or one-dimensional disorder, in which each successive crystal-packing layer is displaced laterally relative to the one below it. A model for the twinning and an algorithm for detwinning the data are described. It is known from other work that when the HslU hexamer binds its cognate protease HslV, the carboxy-terminal helices of HslU protomers distend and bind between HslV subunits. Comparison of HslU alone with its structure in the HslUV complex reveals several conserved amino-acid residues whose side-chain interactions differ between the two structures, suggesting that they may be part of a conformational switch that facilitates the release of the HslU carboxy-terminal helices when HslV binds.

1. Introduction

The HslU protein (heat-shock locus U; Chuang *et al.*, 1993) is a component of a 'prokaryotic proteasome'; in association with its cognate protease, HslV, it selects and delivers polypeptides for proteolytic degradation in an ATP-dependent reaction (Missiakas *et al.*, 1996; Rohrwild *et al.*, 1996; Yoo *et al.*, 1996). HslU is identified at the amino-acid sequence level as a member of the Clp/Hsp100 protein family, members of which have either one (*e.g.* HslU, ClpX) or two (*e.g.* ClpA) ATP-binding domains (for a review, see Schirmer *et al.*, 1996). The Clp/Hsp100 proteins are molecular chaperones whose spectrum of activities demonstrated by *in vitro* experiments include (i) presentation of various substrates to cognate proteases for degradation, *e.g.* the cell-division inhibitor SulA is degraded by HslUV (Seong *et al.*, 1999), SsrA-tagged polypeptides are degraded by ClpXP and ClpAP (Gottesman *et al.*, 1998) and RepA protein is degraded by ClpXP (Pak *et al.*, 1999), (ii) suppression of aggregation, for example, HslU can suppress aggregation of SulA (Seong *et al.*, 2000) and (iii) disassembly of oligomeric complexes, *e.g.* MuA transposase–DNA complexes by ClpX (Levchenko *et al.*, 1995), RepA dimers by ClpA (Pak *et al.*, 1999).

Structures of *E. coli* HslU with protomers having either ATP or SO_4^{2-} in the nucleotide-binding pocket (PDB code 1do0; resolution 3.0 Å) as well as with AMPPNP bound (PDB code 1do2; resolution 4.0 Å) have been reported (Bochtler *et al.*, 2000). They reveal the overall three-domain structure and tertiary fold of HslU: an amino-terminal ATP-binding domain of approximately 210 residues (called the 'N domain'), a

carboxy-terminal domain of about 110 residues (the 'C domain') and an intermediate domain ('I domain') of approximately 120 residues which protrudes from the N domain and which is generally poorly ordered in crystals. They also reveal the 'hexameric ring' quaternary structure of HslU and show that HslU can 'flex' about a hinge between the N and C domains, resulting in subtle changes of the overall conformation of the hexamer ring. A structure for *E. coli* HslU–AMPPNP in a complex with HslV has also been reported (PDB code 1doo; resolution 2.8 Å; Bochtler *et al.*, 2000); in this complex, the overall structure of the HslU protomer shows minimal difference from its structure in HslU alone. These structures show the detailed molecular interaction of *E. coli* HslU with nucleoside triphosphates and one possible mode of assembly of the HslUV complex.

The structure of *H. influenzae* HslUV chaperone–protease complex, with ATP bound to HslU, has also been reported (PDB code 1g3i; resolution 3.4 Å; Sousa *et al.*, 2000); comparison of the polypeptide backbone of HslU in the HslUV complex with that of uncomplexed *H. influenzae* HslU reveals a conformational transition in which the carboxy-terminal helix of HslU distends and binds between subunits of the HslV dodecamer. Here, we report the structure of the *H. influenzae* HslU–ADP complex at 2.3 Å resolution and discuss the features of the structure that may relate specifically to the conformational transition that the molecule undergoes when it forms a complex with HslV.

The crystals in which this HslU structure was solved manifest an unusual twinning or 'one-dimensional disorder' phenomenon. This type of twinning arises from successive planar layers in a crystal shifting laterally into any of several alternative configurations when packing on top of one another; it has a propensity to occur in cases where side-to-side packing interactions within layers of a crystal are strong but stacking interactions between layers are weak. The twinning is not detectable by standard tests for merohedral twinning (Yeates, 1988) and is not readily addressed with crystallographic programs that are readily available. We describe the twinning and its effect on the diffraction intensities, as well as a method for computationally 'detwinning' the data.

2. Experimental

2.1. Protein expression, purification and crystallization

A plasmid for recombinant expression of *H. influenzae* HslU was constructed from an expression plasmid for the HslVU operon described previously (Sousa *et al.*, 2000) as follows. The original plasmid has an *Nde*I restriction site (CAT**ATG**) at the 'start' codon (bold) of HslV. A second *Nde*I site was introduced at the HslU start codon using the Stratagene 'Quik-change' mutagenesis method. The resulting plasmid was digested with *Nde*I and religated to yield a plasmid expressing HslU alone.

Expression of native HslU protein from this plasmid was induced with 0.4 m*M* isopropyl-β-D-thiogalactoside (IPTG) in *E. coli* BL21(DE3) cells at 310 K. Protein was extracted from cells by French press and purified by gravity-flow chromatography on Q-Sepharose [conditions: starting buffer, 0.2 *M* KCl, 5 m*M* β-mercaptoethanol (β-ME), 5 m*M* $MgCl_2$, 0.5 m*M* PMSF, 1 m*M* EDTA, 20 m*M* potassium phosphate pH 7.0 (buffer *A*) plus protease inhibitors; gradient, 0.2→0.5 *M* KCl; HslU protein elutes around 0.35 *M* KCl], followed by FPLC gel filtration on Superdex 200 [Pharmacia; conditions, 0.1 *M* KCl, 5 m*M* β-ME, 1 m*M* $MgCl_2$, 20 m*M* potassium phosphate pH 7.0 (buffer *B*)].

Expression of seleno-L-methionine (SeMet) labeled HslU protein was carried out in the methionine auxotroph *E. coli* strain B834(DE3) (Novagen). Freshly transformed cells were grown at 310 K to an A_{600} of 0.4 in M9 medium supplemented with 10% Luria broth (LB) and 100 µg ml^{-1} ampicillin. Cells were then centrifuged, washed twice with 1.25 × M9 medium and then resuspended and grown to an A_{600} of ∼1.0 at 310 K in M9 medium supplemented with 0.4% glucose, 2 m*M* $MgSO_4$, 0.1 m*M* $CaCl_2$, 0.01 mg ml^{-1} thiamine, 0.04 mg ml^{-1} SeMet, 0.4 m*M* IPTG and 100 µg ml^{-1} ampicillin. SeMet-labelled HslU protein was purified by the same protocol as used for wild-type protein. Comparison of native and SeMet-labelled HslU protein by mass spectrometry revealed essentially complete incorporation of SeMet.

HslU protein was crystallized at 291 K using polyethylene glycol monomethyl ether of average molecular weight 2000 (PEG-MME_{2000}) as precipitant. Native HslU protein, at a concentration of 16–20 mg ml^{-1} in buffer *B* plus 7 m*M* ADP, was crystallized in hanging drops using a precipitant solution consisting of 10% PEG-MME_{2000}, 0.38 *M* $LiSO_4$, 4 m*M* $MgSO_4$, 6% MPD, 100 m*M* tricine pH 7.3. After crystals reached their final size (approximately 0.6 × 0.6 × 0.1 mm in 2 d), the concentration of PEG-MME_{2000} in the well was increased to 16%. The diffraction properties of the crystals were sensitive to divalent and trivalent cations and were improved by the presence of sulfate. SeMet-labeled HslUV protein in buffer *B* plus 10 m*M* ADP was crystallized from a precipitant solution consisting of 10% PEG-MME_{2000}, 0.6 *M* $LiSO_4$, 6% ethanol, 10 m*M* $MgSO_4$, 1 m*M* $ZnSO_4$, 3 m*M* $EuCl_3$ and 100 m*M* tricine pH 7.3. Space-group and unit-cell parameters for these crystals, as well as for two crystals soaked in heavy-atom compounds, are summarized in Table 1.

For data collection, the concentration of MPD in the native HslU crystal stabilization solution was increased from 10 to 30% in 5% increments and 10–20 min intervals; the crystal was then flash-frozen in a stream of nitrogen gas at ∼100 K. Native diffraction data were collected on beamline 9-2 of the Stanford Synchrotron Radiation Laboratory (SSRL) at a wavelength of 1.000 Å. The crystal diffracted anisotropically, showing measurable data to ∼2.0 Å along the a^* and b^* reciprocal axes, but only to ∼2.8 Å along c^*. Data were recorded on Quantum IV CCD detectors and processed with the programs *HKLVIEW*, *DENZO* and *SCALEPACK* (Otwinowski & Minor, 1997). Data-collection statistics are summarized in Table 2.

Data were also collected from a SeMet-labeled HslU crystal. In this case, cryoprotection was performed by briefly

Table 1
HslU crystals and unit-cell parameters.

Crystal	Space group	Unit-cell parameters (Å, °)	Comments
1. Native	*P*622	a = 110.62, c = 335.83	Cryoprotectant: 30% MPD
2. SeMet	*P*622	a = 109.92, c = 314.12	Cryoprotectant: mineral oil
3. $EuCl_3$ heavy-atom soak	*P*1	a = 110.22, b = 110.42, c = 317.18, α = 92.0, β = 92.9, γ = 120.3	Soaked in mother liquor plus 10 m*M* $EuCl_3$ then cross-linked with glutaraldehyde; then adapted to 20% glycerol
4. K_2PtCl_6 heavy-atom soak	*P*1	a = 110.22, b = 109.66, c = 318.12, α = 79.7, β = 94.8, γ = 119.6	Soaked in mother liquor plus 10 m*M* K_2PtCl_6 then cross-linked with glutaraldehyde; then adapted to 20% glycerol

transferring the crystal directly from its stabilization solution to mineral oil (Mallinckrodt) and then flash-freezing as described above. Originally, multiwavelength anomalous dispersion (MAD) data were collected on SSRL beamline 1-5 to a resolution limit of ∼2.8 Å at wavelengths 0.97958, 0.97999 and 1.06883 Å for the selenium absorption peak, dispersive edge and remote energies, respectively, and processed as described above. Although originally collected for *de novo* phasing, the selenium sites determined from these data were ultimately used to verify the HslU structure solved by molecular replacement, as described below; additionally, since the *c* axis of the unit cell of this crystal is ∼22 Å shorter than that of the native crystal, the SeMet-HslU model was refined in order to compare the HslU structures in the two crystals. Data-collection statistics are summarized in Table 2.

2.2. Structure determination

The structure of the *H. influenzae* HslU was solved by molecular replacement with a model of the *E. coli* HslU protein (PDB code 1do0; Bochtler *et al.*, 2000). The hexagonal HslU crystals are twinned (as described in detail below); however, it was possible to carry out the initial steps of molecular replacement and refinement on raw data. Candidate molecular-replacement solutions were identified with the program *AMoRe* (Navaza, 1994) using a single HslU protomer as a search model. Subsequent molecular refinement was carried out with the program package *CNS* (Brunger *et al.*, 1998); rigid-body refinement of the single *E. coli* HslU protomer resulted in $R_{\rm cryst}$ = 0.430, $R_{\rm free}$ = 0.469. The amino-acid sequence of the model was replaced with that of the *H. influenzae* HslU protein. Several segments of polypeptide which could not be traced in the initial $2F_o - F_c$ maps (residues 85–95, 105–245 and 265–272) were deleted. Data were 'detwinned' by the procedure described in §3 and several cycles of model building and refinement were carried out. Clear density for an ADP molecule in the *anti* conformation became apparent in the $2F_o - F_c$ and $F_o - F_c$ maps and was included in the model. Another strong peak in the maps was interpreted as a sulfate ion in an intermolecular contact region. The final native HslU model includes residues 2–87, 92–120, 226–267, 270–444, 94 H_2O molecules, one ADP molecule and one sulfate ion. Final refinement statistics are summarized in Table 2. This structure was used as a starting model for refinement against the SeMet-HslU data, as well as for solving the structure of HslU in the HslUV complex (Sousa *et al.*, 2000). The SeMet-HslU structure was solved using essentially the same protocol as for the native HslU structure. Final refinement statistics are summarized in Table 2.

Table 2
Crystallographic data-collection and refinement statistics.

Values in parentheses refer to the last resolution shell.

	Native HslU	SeMet HslU
Data collection		
Wavelength (Å)	1.00	0.97999
Resolution range (Å)	30–2.30 (2.34–2.30)	40.0–2.80 (2.85–2.80)
Total observations	168887	190830
Unique observations	53223	25899
Completeness (%)	96.5 (95.3)	90.5 (61.3)
Average I/σ	15.4 (8.5)	8.3 (4.8)
$R_{\rm sym}$†	0.058 (0.124)	0.112 (0.305)
Refinement		
Resolution range (Å)	30–2.30 (2.44–2.30)	40.0–2.80 (2.93–2.80)
$R_{\rm cryst}$‡	0.263 (0.387)	0.249 (0.458)
$R_{\rm free}$	0.276 (0.394)	0.256 (0.450)
No. of reflections		
Working set	44585	38890
Test set	4983	4235
No. of protein atoms	2726	2723
No. of solvent/hetero atoms	96 H_2O, 1 ADP, 1 SO_4^{2-}	1 ADP, 1 SO_4^{2-}
Average B values (Å^2)		
Main-chain atoms	44.2	56.8
All atoms	46.2	58.6
R.m.s.d.s		
Bond lengths (Å)	0.008	0.008
Angles (°)	1.24	1.23

† $R_{\rm sym} = \sum |I_{hkl} - \langle I_{hkl}\rangle| / \sum \langle I_{hkl}\rangle$, where I_{hkl} is a single value of the measured intensity of the hkl reflection and $\langle I\rangle$ is the mean of all measured value intensities of the hkl reflection. ‡ $R_{\rm cryst} = \sum |F_{\rm obs} - F_{\rm calc}| / \sum F_{\rm obs}$, where $F_{\rm obs}$ is the observed structure-factor amplitude and $F_{\rm calc}$ is the structure factor calculated from the model. $R_{\rm free}$ is computed in the same manner as $R_{\rm cryst}$ using the test set of reflections.

3. Results and discussion

3.1. Native Patterson peaks suggest crystal twinning

The unit-cell parameters of our native HslU crystals are consistent with a primitive hexagonal space group. The integrated intensities merge with *P*6/*mmm* Laue symmetry and have apparent systematic absences for l = odd along the c* reciprocal axis. These data are consistent with space group $P6_322$. The *H. influenzae* HslU protein forms a stable hexamer in solution (it runs as an ∼300 kDa oligomer by gel filtration; data not shown); additionally, electron-microscopy studies (Kessel *et al.*, 1996; Rohrwild *et al.*, 1997) and, more recently, crystallographic studies (Bochtler *et al.*, 2000) reveal a hexameric ring quaternary structure with diameter ∼110 Å for the closely related *E. coli* HslU protein. The native unit-cell volume could accommodate four HslU hexamers, which for $P6_322$ symmetry would imply two protomers per asymmetric unit. However, native Patterson maps do not show peaks that would result from non-crystallographic symmetry of allowed

crystal-packing arrangements of four hexamers in space group $P6_322$. Instead, peaks of height approximately one-sixth the origin peak are seen in the $w = 0.5$ plane, displaced from the sixfold axis (Fig. 1*a*). More precisely, if we define x_0 to be the magnitude of the displacement of the Patterson peaks from the sixfold axis, then peaks are observed with coordinates $(u, v, w) = (x_0, 0.0, 0.5)$ and equivalent positions generated by the sixfold rotational symmetry, *i.e.* $(x_0, x_0, 0.5)$, $(0.0, x_0, 0.5)$, $(-x_0, 0.0, 0.5)$, $(-x_0, -x_0, 0.5)$, $(0.0, -x_0, 0.5)$. It is notable that the value of x_0, the magnitude of the displacement of the peaks from the sixfold axis of the Patterson, varies from one crystal to another – we have observed values from 0.20 to 0.23.

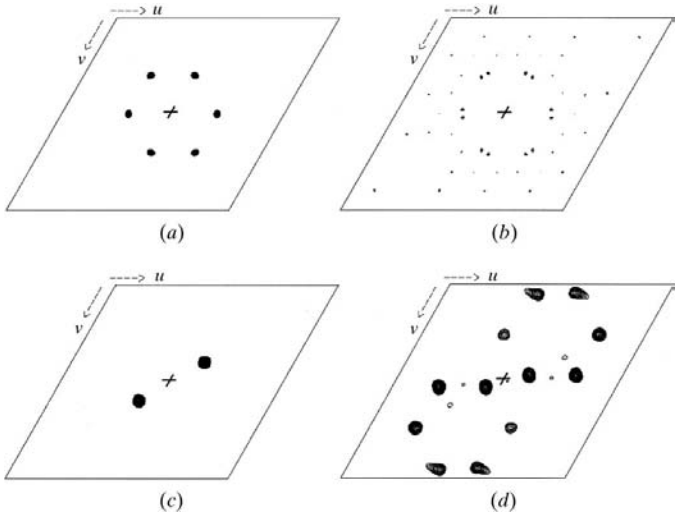

Figure 1
$w = 0.5$ sections of Patterson maps for HslU crystals. In each case, extent is (–0.5, 0.5) in u and v; (0, 0, 0.5) is at the center of the section. (*a*) Hexagonal native HslU computed from experimental intensities (crystal 1 in Table 1). (*b*) Native HslU computed from 'detwinned' intensities. (*c*) Triclinic crystal resulting from $EuCl_3$ heavy-atom soak (crystal 3 in Table 1). (*d*) Triclinic crystal resulting from K_2PtCl_6 heavy-atom soak (crystal 4 in Table 1).

The native Patterson is consistent with the crystal packing scheme shown in Fig. 2.

(i) In solution, HslU forms a stable hexameric 'ring'. In the crystals, two rings pack together to form a 'crystal-packing dodecamer' that has 622 point-group symmetry. (The description of the packing is more easily described and visualized as packing of dodecamers rather than hexamers, even though the dodecameric quaternary structure is a product of the crystal packing.)

(ii) HslU dodecamers pack into well ordered planar layers through side-by-side interactions. The side-by-side packing is stabilized by sulfate ions, which bridge pairs of HslU protomers (Fig. 2*b*). The layers have hexagonal $P622$ symmetry.

(iii) When a second layer packs on top of the first, it is displaced laterally and parallel to the plane of the first layer by $(x_0, 0)$, where typically $x_0 \simeq 0.22$ in fractional coordinates, or by translations that are equivalent by the hexagonal symmetry of the first layer, *i.e.* (x_0, x_0), $(0, x_0)$, $(-x_0, 0)$, $(-x_0, -x_0)$ or $(0, -x_0)$ (referenced to a hexagonal lattice) (Fig. 2*c*).

(iv) There are two alternative schemes that can then give rise to the Patterson peaks we observe, as shown in Fig. 2(*d*). (*a*) The second layer is displaced horizontally by $(x_0, 0)$ relative to the first. If the third shifts in the opposite direction $(-x_0, 0)$, then it will be directly above the first layer. The crystal can be built up of macroscopic domains with long-range correlation between alternating layers, such that the third, fifth, ..., layers stack directly above the first and the fourth, sixth, ..., layers stack directly above the second. The translational repeat in the vertical direction is equal to the thickness of two layers, ~330 Å in the HslU crystals. The twinning we observe would then result if macroscopic crystal domains in the crystal were rotated by multiples of 60° around the c axis relative to each other, in such a manner that each orientation was sampled equally. This can be thought of as merohedral twinning with six alternative orientations of crystal domains, differing by their rotation around the hexagonal axis. (*b*) Alternatively, if the selection of the displacement from the six alternatives in each successive layer is random, then there would be no long-range correlation in the stacking of layers. Both of these schemes can give rise to apparent primitive hexagonal symmetry in the diffraction data, as well as to the translation peaks we observe in the $w = 0.5$ layer of native Pattersons.

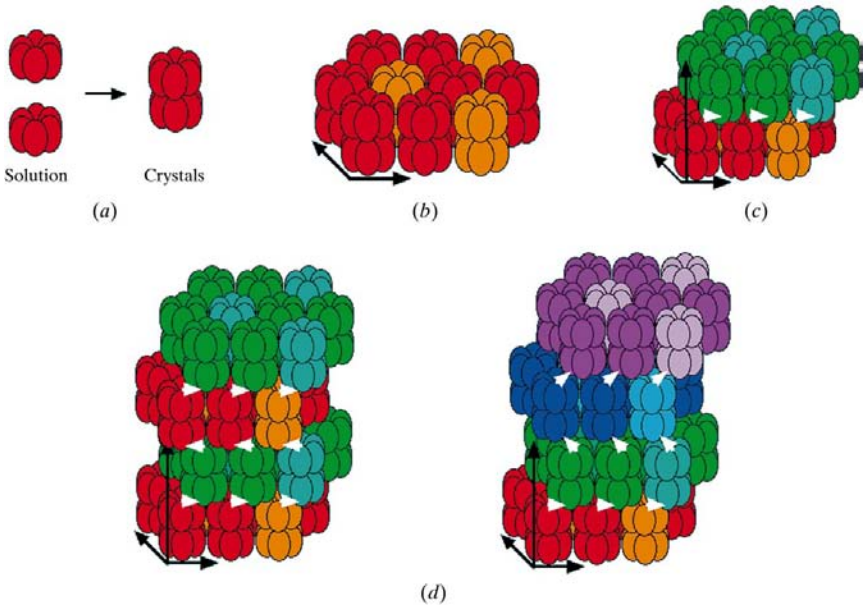

Figure 2
Model for HslU crystal twinning. Ellipsoids represent individual HslU protomers. Contrasting colors are used in planar arrays for clarity. Vectors that are parallel to the crystallographic unit-cell axes are shown for reference in (*b*)–(*d*). (*a*) Two HslU hexamers pack in crystals to form a 'dodecamer' with 622 symmetry. (*b*) HslU dodecamers pack side-to-side to form layers with hexagonal symmetry. (*c*) Each layer is shifted laterally relative to the layer beneath it. (*d*) Successive layers may stack on top of each other either with the direction of lateral shifts being correlated (left) or with the direction of lateral shifts being random (right).

In the HslU crystals, this packing scheme arises as a consequence of the lability of the intermolecular packing interactions between planar layers. (The molecular basis for this is described later.) The lability of these interactions is illustrated further by crystals soaked in heavy-atom compounds; in some (rare and irreproducible) cases, we observe transitions to triclinic symmetry, with unit-cell parameters closely related to those of the hexagonal form (Table 1). Native Patterson $w = 0.5$ sections are shown in Figs. 1(*c*) and 1(*d*) for two examples. The section in Fig. 1(*c*) shows a single peak per asymmetric unit; the height is 40% (*i.e.* approximately half) of the origin peak which would result from a single translation vector relating one dodecamer to the other in a triclinic unit cell encompassing two dodecamers. The Patterson section in Fig. 1(*d*) shows six peaks of unequal magnitude, which would arise from a more complex packing scheme in which successive layers are displaced by any of several different translation vectors of unequal weight.

3.2. Crystal twinning model accounts for Patterson peaks and distribution of intensities

In a simplistic analysis of the model of crystal twinning described above, we consider only nearest-layer contributions to the scattering. The experimental intensities will then have six contributions of equal weight from each of the six allowed lateral translation of the second layer relative to the first. The contribution of one HslU crystal-packing dodecamer to the structure factor can be defined as $F_0(\mathbf{h})$,

$$F_0(\mathbf{h}) = \int_{\text{HslU dodecamer}} \rho(\mathbf{x}) \exp(2\pi i \mathbf{h} \cdot \mathbf{x})\, \mathrm{d}^3x, \qquad (1)$$

where $\mathbf{h} = (h, k, l)$, the Miller indices of the reflection, $\mathbf{x} = (x, y, z)$, the fractional coordinates of the position in the unit cell, and $\rho(\mathbf{x})$ is the scattering density. Then, the combined contribution of this dodecamer and a second one related by a general translation $\mathbf{t} = (x_0, y_0, z_0)$, in fractional coordinates, will be

$$F_{\text{both}}(\mathbf{h}) = [1 + \exp(2\pi i \mathbf{h} \cdot \mathbf{t})] F_0(\mathbf{h}). \qquad (2)$$

The calculated intensity for this pair of dodecamers will be

$$I_{\text{both}}(\mathbf{h}) = 4[\cos^2(\pi \mathbf{h} \cdot \mathbf{t})] I_0(\mathbf{h}), \qquad (3)$$

where $I_0(\mathbf{h})$ would be the intensity for a single dodecamer. In the special case that the z value of the translation is exactly 1/2, *i.e.* $\mathbf{t} = (x_0, y_0, 0.5)$, the cosine term reduces to

$$\begin{aligned} &\cos^2 \pi(hx_0 + ky_0) \quad \text{for } l = \text{even} \\ &\sin^2 \pi(hx_0 + ky_0) \quad \text{for } l = \text{odd}. \end{aligned} \qquad (4)$$

For the HslU crystals, the net intensity of a reflection will have six contributions, one from each of the six alternative translations observed in native Pattersons: $(x_0, 0, 0.5)$, $(x_0, x_0, 0.5)$, $(0, x_0, 0.5)$, $(-x_0, 0, 0.5)$, $(-x_0, -x_0, 0.5)$ and $(0, -x_0, 0.5)$, in fractional coordinates referenced to a hexagonal axis system. Summing the trigonometric terms for each of these contributions and weighting each contribution by 1/6 gives the net intensity of a reflection, $I_{\text{total}}(\mathbf{h})$,

$$\begin{aligned} I_{\text{total}}(\mathbf{h}) &= \frac{4}{3}[\cos^2 \pi h x_0 + \cos^2 \pi(h + k)x_0 + \cos^2 \pi k x_0] I_0(\mathbf{h}) \\ &\qquad \text{for } l = \text{even} \\ I_{\text{total}}(\mathbf{h}) &= \frac{4}{3}[\sin^2 \pi h x_0 + \sin^2 \pi(h + k)x_0 + \sin^2 \pi k x_0] I_0(\mathbf{h}) \\ &\qquad \text{for } l = \text{odd}. \end{aligned} \qquad (5)$$

This model for the twinning predicts that the ratio of the average intensity for the l = odd reflections to the l = even reflections will follow the ratio of the sine term to the cosine term in the expressions above; Fig. 3 compares the ratio of the average measured intensities with the calculated ratio expected from this model for the (hk0) plane of reciprocal space. The model predicts systematic absences for l = odd reflections along the c^* reciprocal axis, as can be seen by substituting $h = k = 0$ into (5) above; this is consistent with the systematic absences we observe in our experimental data.

This analysis of the twinning is exact for a case in which there is long-range correlation of the lateral shifts of packing layers, but only approximate for the case in which the directions of successive lateral shifts are uncorrelated/random. Analysis of the latter case requires inclusion of the contributions of successive layers throughout the crystal to the structure factor, with all possible displacements of each layer weighted according to their probability in a statistical distribution of the displacements. Analysis of this type of statistical, or one-dimensional, disorder for the specific case of two alternative packing arrangements has been discussed by Wilson (1949) and has also been documented and analyzed for crystals of 'statistically orthorhombic' imidazole-methemo-

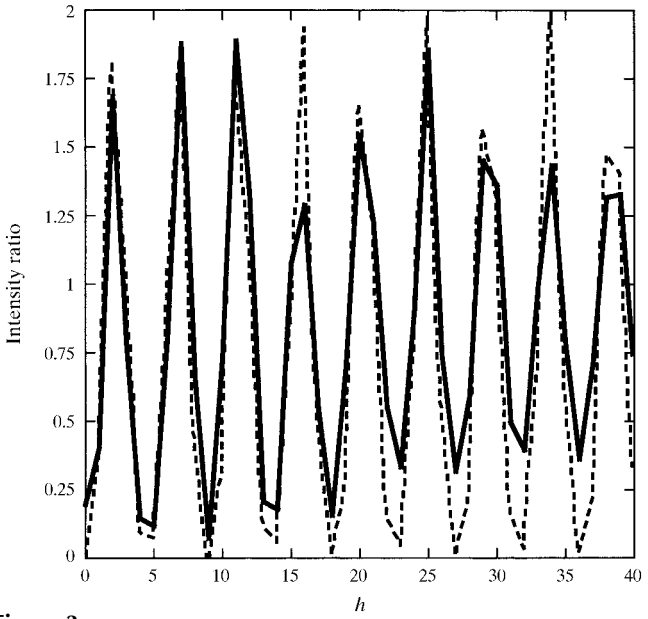

Figure 3
Ratio of average intensities for l = odd reflections to l = even reflections in the ($h0l$) plane of native HslU crystal. Solid line: ratio of experimental intensities. Dotted line: computed as $(2\sin^2\pi h x_0)/(2\cos^2\pi h x_0 + 1)$, the ratio of the sine and cosine terms in (5), for the particular case of $k = 0$ with $x_0 = 0.221$.

Table 3
Comparison of refinement statistics between detwinned and raw data for several crystals.

For native and SeMet crystals, the molecular models were built and refined against detwinned data; the models were then put through several cycles of minimization against raw data. For other crystals, the native model was adjusted through several rounds of minimization against both raw and detwinned data without manual rebuilding. R_{cryst} and R_{free} are defined in Table 2.

		Detwinned data		Raw data		Difference		
Crystal	Resolution (Å)	R_{cryst}	R_{free}	R_{cryst}	R_{free}	R_{cryst}	R_{free}	Patt. peak†
Native	2.3	0.267	0.275	0.300	0.287	0.033	0.012	0.106
SeMet	2.8	0.243	0.257	0.302	0.323	0.059	0.066	0.150
Cryst. 25 $LuSO_4$ soak	3.0	0.271	0.270	0.317	0.311	0.046	0.041	0.133
Cryst. 37 native	2.6	0.265	0.268	0.309	0.338	0.036	0.070	0.144
Cryst. 33 TAMM soak	3.5	0.293	0.261	0.305	0.255	0.012	0.006	0.090
Test data‡	3.0	0.192	0.214	0.312	0.346	0.120	0.132	0.164

† Patt. peak = height of peak in $w = 0.5$ section relative to the origin peak of 1.0. ‡ Test data were generated as described in the text.

globin (Bragg & Howells, 1954; Cochran & Howells, 1954; Howells & Perutz, 1954). A similar statistical disorder has been suggested for a crystal form of erythrocyte catalase (Glauser & Rossmann, 1966).

The HslU diffraction patterns have symptoms that suggest the extent of long-range correlation of layer packing may vary from crystal to crystal. One characteristic of the statistical disorder is that certain classes of reflections are broadened along the reciprocal-space direction perpendicular to the packing layers; the lower the correlation in packing of successive layers, the greater the broadening of the reflections (Wilson, 1949). In the HslU crystals, this results in broadening of reflections in the c^* reciprocal direction. The magnitude of the broadening varies from one crystal to another; since this is in the direction of the $(\sim 330\ \text{Å})^{-1}$ reciprocal spacing, it often results in overlap of neighboring reflections and defeats data processing. In addition, we have occasionally found crystals whose diffraction patterns include a well defined $(\sim 660\ \text{Å})^{-1}$ reciprocal spacing in the c^* direction, which is further evidence of a breakdown of long-range correlation in the stacking of the layers in the crystal. In this context, the correction we apply to our experimental intensities, described below, should be regarded as a first approximation rather than an exact correction.

3.3. Correction of the diffraction data for twinning and its effect on model refinement

Test calculations demonstrate that the twinning model described above reproduces the peaks observed in the $w = 0.5$ section of the native HslU Patterson. We have also considered and carried out test calculations for an alternative 'partial occupancy' model. Specifically, we (i) generated a dodecamer with full occupancy centered at the origin and six additional dodecamers, each with an occupancy of 1/6, centered at (0.221, 0, 0.5) and the five symmetry-equivalent positions generated by the sixfold rotation around the c axis; (ii) computed structure factors for the entire assembly; (iii) calculated a Patterson map from the absolute square of the structure factors. This models the twinning as resulting from random displacements of individual dodecamers in the second layer relative to those in the first, rather than a concerted displacement of the second planar layer relative to the first. In this case, the peaks in the $w = 0.5$ plane of the Patterson do not appear; by implication, the twinning cannot be attributed to random alternative positions of dodecamers in the second layer. By implication, the options for addressing multiple conformations that are incorporated in standard programs for heavy-atom phasing and model refinement will not account for the twinning.

To address this problem, we have 'detwinned' the experimental intensity measurements. Using (5), we see that dividing $I_{total}(\mathbf{h})$ by the cosine term in brackets (for l even reflections) or the sine term (for l odd reflections) give $I_0(\mathbf{h})$, the contribution of a single HslU dodecamer centered at the origin to the intensity of the reflection,

$$I_0(\mathbf{h}) = \frac{3}{4[\cos^2 \pi h x_0 + \cos^2 \pi (h+k) x_0 + \cos^2 \pi k x_0]} I_{total}(\mathbf{h}) \quad \text{for } l = \text{even}$$

$$I_0(\mathbf{h}) = \frac{3}{4[\sin^2 \pi h x_0 + \sin^2 \pi (h+k) x_0 + \sin^2 \pi k x_0]} I_{total}(\mathbf{h}) \quad \text{for } l = \text{odd}. \tag{6}$$

After detwinning of the data, the unit cell and space group remain unchanged, but the intensities correspond to the contribution of a single HslU protomer in the asymmetric unit. The $w = 0.5$ section of the native Patterson computed with detwinned data is shown in Fig. 1(*b*); the major peak at (0.221, 0, 0.5) is no longer present. (It is notable, however, that several other minor peaks appear in this section, suggesting that this procedure is not completely correcting for the twinning; we discuss this point in more detail below.)

In the computational procedure, each intensity and standard deviation are multiplied by a detwinning factor derived from (6) above. (For purposes of both computation and discussion it is convenient to ignore the factor of 4 in the denominator; the detwinning factor then has a minimum value of 1.0 rather than 0.25.) Since the cosine and sine terms in the denominators of (6) can approach or equal zero for some values of h, k and x_0, it is necessary to impose an upper bound on the allowed value of the detwinning factors. With an upper bound in the range 20.0–50.0, approximately 7% of the intensities are omitted because the computed correction exceeds the bound; with an upper bound of 10.0, approxi-

mately 8% are rejected. Systematic comparisons show that numerically smaller upper bounds, which omit more reflections, give better refinement statistics; for example, for the native data, R_{free} improves from 0.287 to 0.278 when the upper bound on the detwinning factor is reduced from 50.0 to 10.0. We presume this reflects the fact that in this procedure many weak intensities are multiplied by large numerical factors, so that many of the large amplitudes used in the subsequent refinement have intrinsically large errors; setting a rejection level of 50.0 *versus* 10.0, although it only increases the number of data used in refinement by ∼1%, introduces amplitudes that are large in magnitude but low in precision.

The effects of the detwinning on the refinement statistics were compared for several crystals; the results are summarized in Table 3. When compared with raw data, refinement against detwinned data typically improves the crystallographic *R* factor by 3–6%. To check whether this trend is reasonable and whether the detwinning procedure works correctly, a comparison was made with test data.

(i) For each of the six alternative displacements of the second dodecamer relative to the first, coordinates were generated for a pair of HslU dodecamers.

(ii) Using the program *SOLVE* (Terwilliger & Berendzen, 1999), structure factors were computed from the atomic coordinates in space group *P*1.

(iii) Intensities were computed from the structure factors, with 6% random noise incorporated into them; then, for each reflection, the intensities and statistical errors of the six configurations were averaged.

(iv) The primitive hexagonal asymmetric unit was extracted from the averaged intensities; this provided our simulated 'raw' data in space group *P*622.

(v) The detwinning protocol was applied to the raw data, giving 'detwinned' data.

(vi) The HslU model which was used to generate the structure factors was subjected to one cycle of refinement in *CNS*, including simulated-annealing, energy-minimization and restrained *B*-factor refinement.

The simulated raw data yielded $R_{cryst} = 0.312$ and $R_{free} = 0.346$, while the detwinned data yielded $R_{cryst} = 0.192$ and $R_{free} = 0.214$, an improvement of 12.0% in the crystallographic *R* factor (13.2% in R_{free}) (Table 3).

The disparity between the final refinement statistics of the test data and the statistics of the experimental data may have

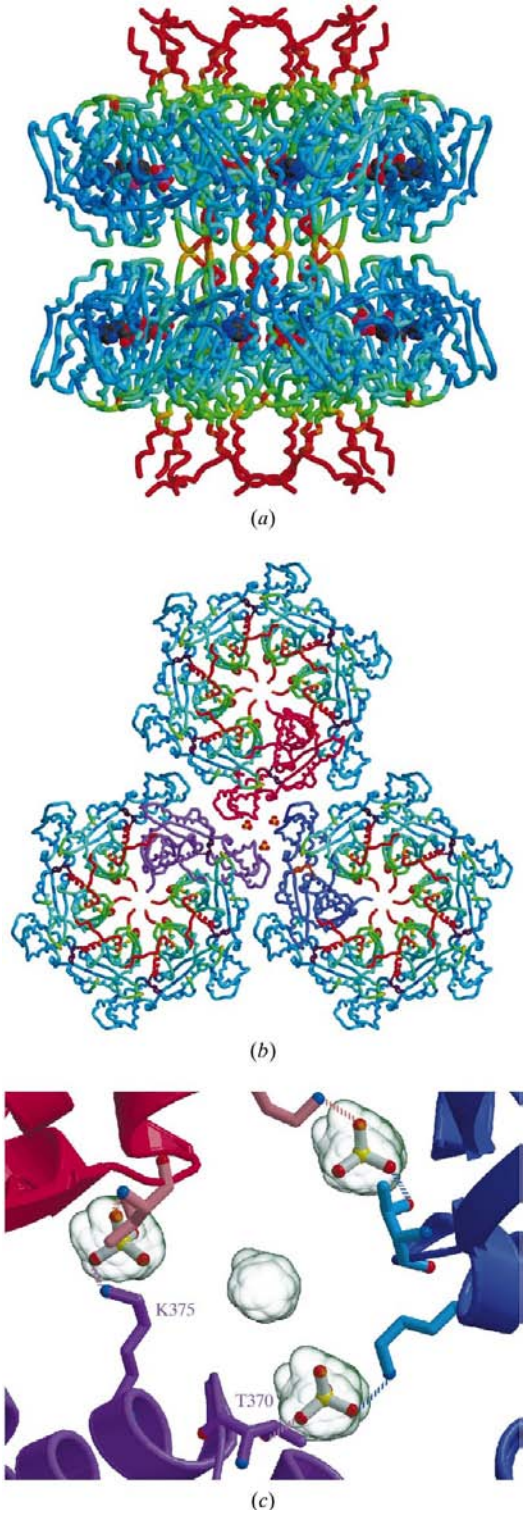

Figure 4
Crystal-packing interactions of HslU. (*a*) Side view of packing of two HslU hexamers to form a 'dodecamer'. HslU protomers are represented with a 'tube' drawing of the backbone, colored by *B* factor from blue (lowest value, 10 Å^2) to red (highest value, 100 Å^2). ADP molecules are shown in a space-filling representation. The N and C domains form hexameric rings that interact at the equator of the complex; the I domains extend vertically from the top and bottom of the complex. (*b*) Packing of three HslU hexamers around a crystallographic threefold axis; top view looking down on a planar layer. Five of the six protomers are colored by *B* factor as in (*a*); the sixth is colored red, magenta or blue in the upper, lower left or lower right hexamer, respectively. Three SO_4^{2-} ions near the threefold axis are shown in space-filling representation. (*c*) Close-up view of the interactions around the threefold axis. Portions of the three HslU protomers that are colored uniformly in (*b*) are shown in ribbon representation. An $F_o - F_c$ omit electron-density map, in which the SO_4^{2-} ion was omitted from the model that was refined and used to compute phases, contoured at 9.5σ is shown in transparent representation. Dashed lines show interactions between HslU residues and the sulfate ions. Figs. 4(*a*), 4(*b*), 6 and 8 were produced with *Molscript* (Kraulis, 1991); Figs. 4(*c*) and 5 were produced with *Bobscript* v.2.4 (Esnouf, 1997, 1999); Figs. 4–6 and 8 were rendered with *Raster3D* v.2.4 (Merritt & Bacon, 1997).

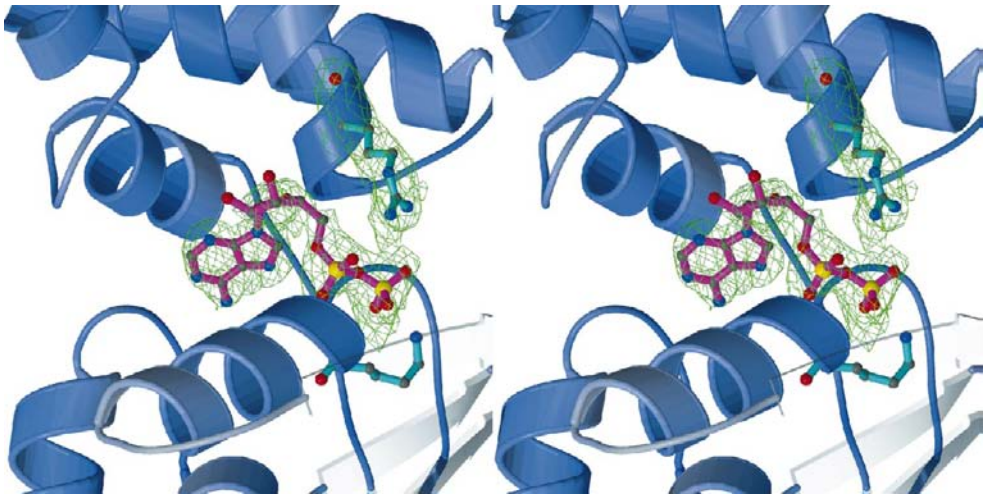

Figure 5
Representative electron-density map around the nucleotide-binding site. Stereoview of a simulated-annealing omit map (green, contoured at 4.2σ) in which ADP and Arg394 were omitted from the model used in refinement. Protein is shown as a ribbon diagram; ADP and residues Arg394 and Lys63 are shown in ball-and-stick representation. Distances from the non-bonded guanidinium N atoms of Arg394 to the nearest phosphate O atom are 2.8 and 2.5 Å; distance from the amino group of Lys63 to the nearest phosphate O atom is 2.8 Å.

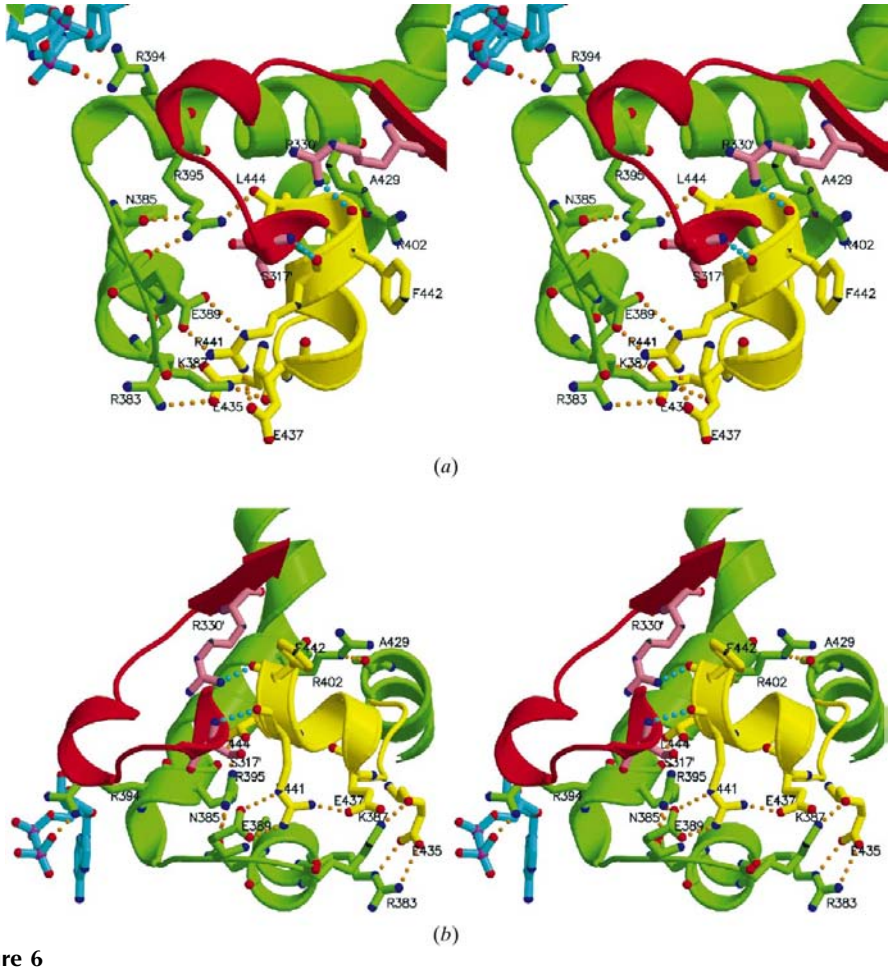

Figure 6
Stereoviews of interactions with the carboxy-terminal helix of the HslU protomer. One HslU protomer is colored green through residue 430 and yellow for residues 431–444; a neighboring HslU protomer is colored red; ADP is colored cyan. Two different views are shown in (*a*) and (*b*).

contributions from two different sources. In the final HslU model, 105 residues representing 23.6% of the scattering density could not be modeled and are absent. In addition, as discussed in §3.2, there are several indications that the crystal twinning may be more complex than the model we use to describe it and, by implication, the detwinning procedure may only partially compensate for it. One indication is the height of the peaks in the w = 0.5 plane of the native Pattersons, which range from 0.090 to 0.144 of the origin peak for the crystals summarized in Table 3; the theoretical value predicted by the twinning model is 0.167 = 1/6 of the origin peak. Further, data sets which show the greatest discrepancy from the ideal value of 0.167 for the Patterson peak also show the smallest improvement in $R_{\rm free}$ for detwinned data compared with raw data in the refinement. Also, the w = 0.5 sections of Patterson maps computed from detwinned data show residual peaks. Deviations from ideality in the translation relating one HslU dodecamer to another in the crystal could give rise to the behavior we observe. However, despite these disparities, the twinning model and detwinning procedure appear to account and correct for the effect of the twinning on the diffraction data to a good approximation.

3.4. Structure of the HslU–ADP complex and its relation to HslUV assembly

The first HslU structure to be reported was that of the *E. coli* protein (Bochtler *et al.*, 2000); that work delineated the folding pattern and three-domain structure of the HslU protomer, as well as the quaternary assembly of the hexamer, with the N and C domains forming a ring and the I domains

extending outward from one face of the ring. The tertiary and quaternary structures of the *H. influenzae* HslU reported here are similar to those of the *E. coli* protein, with which it shares 80% amino- acid sequence identity; the C_α backbone of the *H. influenzae* HslU protomer superimposes on those of *E. coli* protomers from different crystal forms with root-mean-square differences of 0.8–1.0 Å.

The crystal packing of the *H. influenzae* HslU molecules can be described in terms of the molecular structure (Fig. 4). Two HslU hexameric rings pack together with the I domains extending in opposite directions from the complex (Fig. 4*a*), forming the 'crystal-packing dodecamer' with 622 point-group symmetry discussed above. The dodecamers pack into stable planar layers through side-by-side interactions; this packing is stabilized by sulfate ions, which bridge pairs of HslU protomers (Figs. 4*b* and 4*c*). The labile interactions between layers must be mediated through the I domains, which extend from both surfaces of the planar layers; however, since the extremities of these domains are disordered in our crystals, we do not observe the interactions directly.

The *c* axis of the *H. influenzae* SeMet-labelled crystal is 22 Å shorter than that of the native HslU crystal, as a result of using different precipitants and cryoprotectants for the two crystals. Despite this difference, the C_α backbones of the models for the two structures superimpose with a root-mean-square difference of 1.0 Å. We have observed a similar contraction of the *c* axis when crystals are crosslinked with glutaraldehyde (Table 1). We presume that the shrinking of the *c* axis is a consequence of changes in structure and/or intermolecular contacts in the extremities of the I domains, which are disordered in our crystals such that we cannot see the specific changes that take place.

Superposition of structures of HslU protomers from both *E. coli* and *H. influenzae* in different crystal forms shows that there is minimal variation of the structure within the individual N and C domains, that there is significant flexing about the hinge between the N and C domains and that there may be substantial conformational changes in the I domains. HslU undergoes a major conformational change when it binds HslV to form the HslUV complex; most notably, the carboxy-terminal helices of the HslU protomers distend and intercalate between subunits of HslV (Sousa *et al.*, 2000). Additionally, it is hypothesized

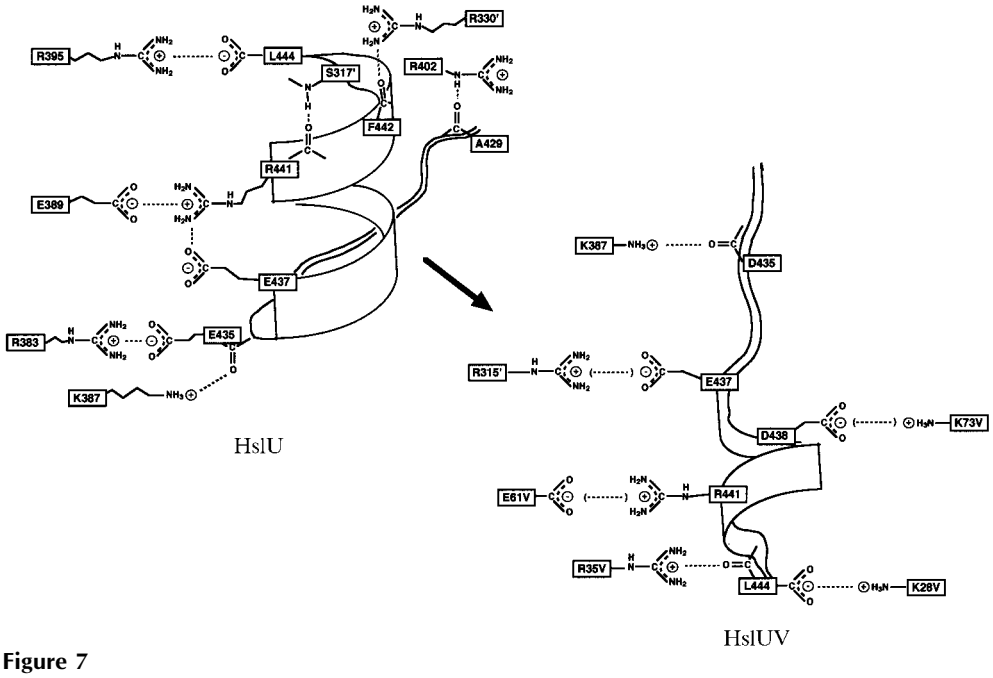

Figure 7
Schematic drawing showing interactions of the carboxy-terminal helix of HslU in the HslU hexamer (left) and in the HslUV complex (right). Residues from neighboring subunits of HslU are denoted with a prime; residues from HslV are denoted with 'V' following the residue number.

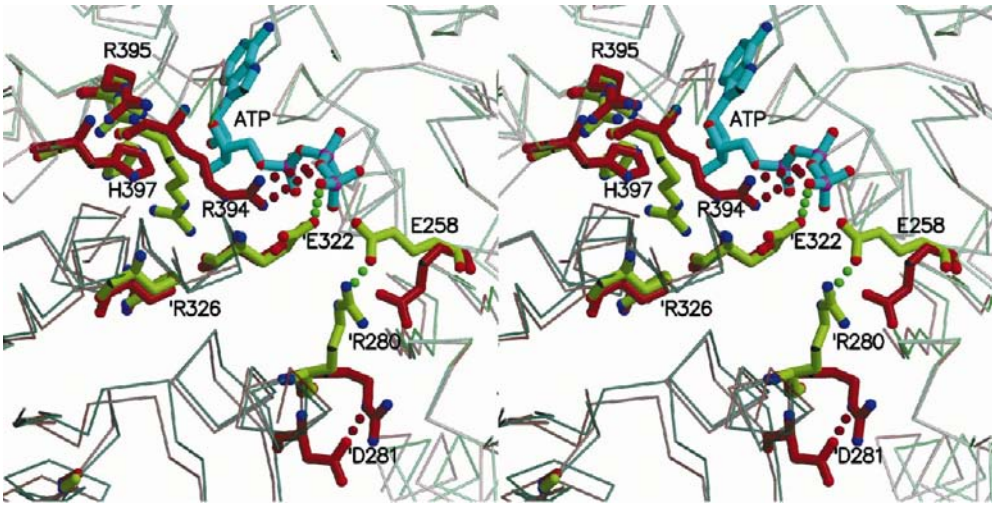

Figure 8
Selected residues and superposition of *H. influenzae* HslU and HslUV structures in the vicinity of the nucleotide-binding pocket. Uncomplexed HslU, reported here, is colored brown; HslU from the HslUV complex is green. Only the ATP from HslUV is shown; for simplicity, the ADP from HslU, which superimposes on ATP, is not included. The backbone of protomer whose ATP is shown has the lighter trace; the backbone of neighboring HslU subunit has the darker trace and residues are denoted with a prime (′).

that in order to denature polypeptides and present them to the interior cavity of the HslV protease, HslU cycles through alternative conformations in a reaction pathway that is coupled to its ATPase cycle. The molecular mechanisms which trigger these conformational transitions are not understood; comparison of uncomplexed *H. influenzae* HslU (with ADP bound) to its structure in the HslUV complex (with ATP bound) suggest several amino-acid residues that may contribute to conformational transitions.

The interactions around both the carboxy-terminal helix and the nucleotide-binding site are well defined in the HslU structure; a representative simulated-annealing omit map, in which ADP and Arg394 were omitted from the model used for refinement and phase calculation, is shown in Fig. 5. The guanidinium group of the side chain of Arg394 forms a well defined salt bridge with the β phosphate of ADP. Molecular interactions with the carboxy-terminal helix and ADP are shown in Fig. 6 and also schematically in Fig. 7. The side chain of Arg395 binds the terminal carboxyl group of the polypeptide. Arg394 and Arg395 are conserved across phylogeny in HslU sequences that are currently known, raising the possibility that they work in concert as a molecular switch in HslUV assembly. There are several other salt bridges and hydrogen-bond interactions stabilizing the position of the carboxy-terminal helix in the HslU structure which are less well conserved across phylogeny, including salt bridges between Arg441 and Glu389, and also between Glu435 and Arg383.

Residues whose side-chain interactions differ between uncomplexed HslU and the HslUV complex are shown in Fig. 8, with their HslU conformations in brown and the conformations from the HslUV complex in green. There is a network of interactions which changes when the HslUV complex forms; most notably, Arg394 from the C domain 'untethers' from the phosphates of the nucleotide bound to the N domain and Arg280 of a neighboring subunit forms a salt bridge with the catalytic Glu258 of the DEID motif in the N domain. Arguably, some of these differences might be attributable to the fact that the HslUV complex has ATP bound, while the uncomplexed *H. influenzae* HslU has ADP bound. However, the equivalent side chains of uncomplexed *E. coli* HslU with AMPPNP are found to be in similar conformations to the *H. influenzae* HslU with ADP bound, favoring the interpretation that the differences we observe result from assembly of the HslUV complex.

In *E. coli* HslU, mutating the residue which corresponds to Arg394 of the *H. influenzae* protein abolishes both the

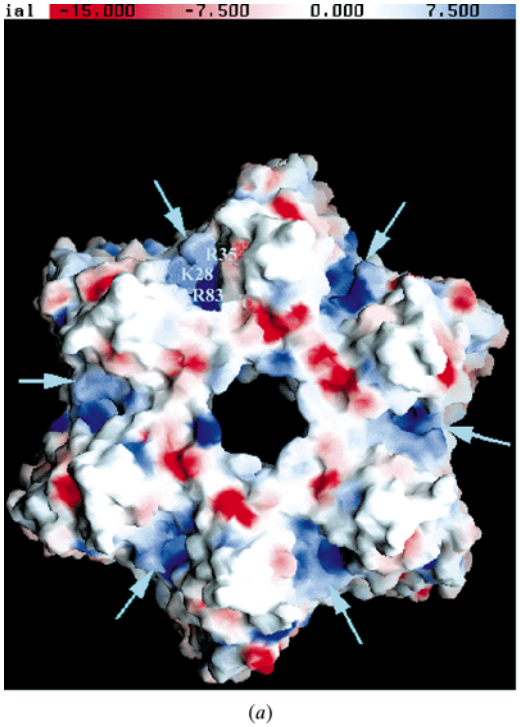

(*a*)

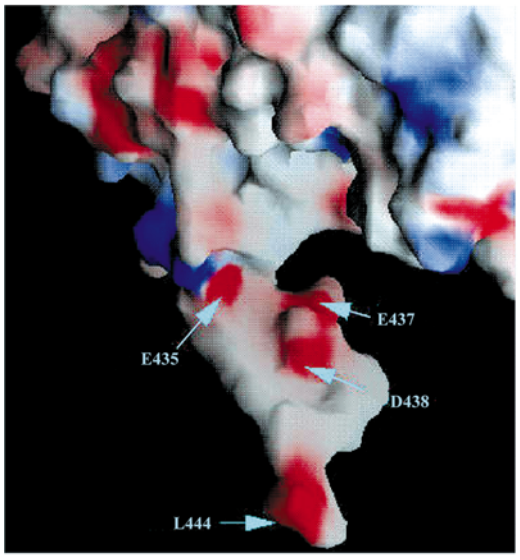

(*b*)

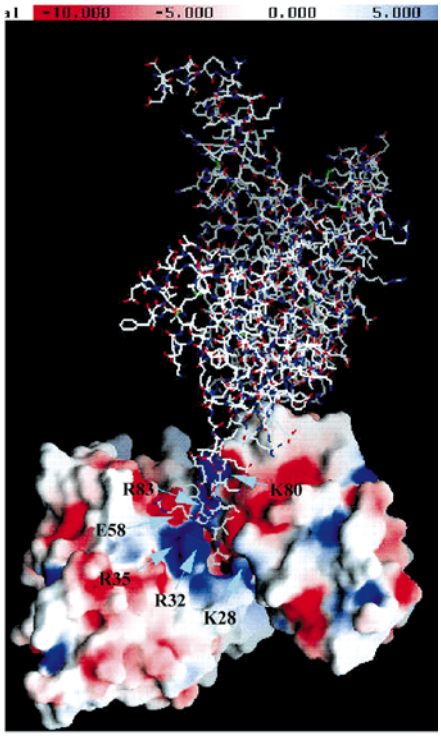

(*c*)

Figure 9
Electrostatic surface potentials of HslV and HslU. Positions of some amino-acid residues are labeled in each figure. (*a*) View looking down the sixfold axis of the HslV dodecamer from the HslUV complex (Sousa *et al.*, 2000). Arrows indicate the electropositive grooves into which the carboxy-terminal helices of HslU intercalate. (*b*) Carboxy-terminal helix of one protomer of HslU in its conformation from the HslUV complex. (*c*) Side view showing the interface between the carboxy-terminal helix of HslU, shown as a ball-and-stick model, and the groove between two HslV protomers. Electrostatic potentials were computed with the program *GRASP* (Nicholls & Honig, 1991), using a dielectric constant of 2.0 for the interior of the protein and 80.0 for the solvent area and an effective ionic strength equivalent to 1.0 *M* salt.

ATPase activity of HslU and the peptidase activity of the HslUV complex on both short peptides and the SulA protein. Mutating the *E. coli* residues equivalent to Glu322 and Arg326, whose side-chain conformations are not altered by HslUV assembly, also abolishes the ATPase and peptidase activities (Song *et al.*, 2000). No data are available on the effect of mutating Arg280. The structural data suggest that Arg280, working in concert with Arg394 and Arg395, may facilitate the release of the carboxy-terminal helix through the conformational shifts we observe which correlate with assembly of the HslUV complex.

Another perturbation which may contribute to destabilizing the interactions with the carboxy-terminal helix, including the salt bridge from Arg395 to the terminal carboxyl group of the polypeptide chain, is the 'flexing' of approximately 3° between the N and C domains of HslU when the complex with HslV forms. At the same time, comparison of structures of *E. coli* HslU protomers with and without AMPPNP bound also reveal significant flexing between the domains, without a concomitant release of the carboxy-terminal helix (Bochtler *et al.*, 2000). Therefore, this perturbation may contribute to but does not by itself define a molecular mechanism for the release of the carboxy-terminal helix that occurs when HslU binds HslV.

Another factor which may contribute to the conformational transition in HslU is the general electrostatic interactions between the HslU hexamer and the HslV dodecamer. An image of the electrostatic surface potential of HslV, computed with the program *GRASP* (Nicholls & Honig, 1991), is shown in Fig. 9(*a*); it is particularly notable that the crevices in which the HslU carboxy termini bind have a strong positive electrostatic potential. Complementary to this, the carboxy terminus of HslU, in its distended conformation, shows a strong electronegative potential (Fig. 9*b*). Also, inspection of the interactions of the carboxy-terminal segment of the HslU polypeptide in the HslUV complex reveals several probable ionic interactions which are consistent with an electrostatic contribution to the binding of the distended helix to HslV in the HslUV complex (Figs. 7 and 9*c*). Thus, electrostatic complementarity may facilitate the structural transition that occurs when HslU binds to HslV.

In summary, the high-resolution structure of the *H. influenzae* HslU–ADP shows that Arg394 and Arg395, which are conserved across phylogeny, 'link' the carboxy terminus in the C domain to ADP bound in the N domain. When the HslUV complex assembles, Arg280 links a neighboring subunit to the nucleotide through interactions with the catalytic residue Glu258, while Arg394 releases from the nucleotide. These residues may constitute a molecular 'switch' which couples ATP binding and hydrolysis, or alternatively initial HslV binding, to release of the carboxy-terminal helix of HslU and formation of the HslUV complex. Other factors which may facilitate release of the helix include (i) destabilization of the interactions holding the carboxy-terminal helix in place when HslU protomers flex about the hinge between the N and C domains and (ii) electrostatic interactions between HslU and HslV, as revealed by the electronegative potential of the carboxy-terminal helix of HslU and the complementary electropositive potential in the helix-binding pocket of HslV.

We thank Dr Sigurd Wilbanks for helpful assistance and advice, Lushen Li for technical assistance, Dr Henry Bellamy and other beamline staff at the Stanford Synchrotron Radiation Laboratory (SSRL) for assistance with data collection, Dr Boaz Shannon for discussions on one-dimensional disorder and bringing the reference by A. J. C. Wilson to our attention, and an anonymous referee for bringing the references on hemoglobin and catalase to our attention. This work was supported by award GM-39928 from the National Institutes of Health (NIH) to DBM. This work is based upon research conducted at SSRL, which is funded by the Department of Energy (BES, BER) and the National Institutes of Health (NCRR, NIGMS).

References

Bochtler, M., Hartmann, C., Song, H. K., Bourenkov, G. P., Bartunik, H. D. & Huber, R. (2000). *Nature (London)*, **403**, 800–805.
Bragg, W. L. & Howells, E. R. (1954). *Acta Cryst.* **7**, 409–411.
Brunger, A. T., Adams, P. D., Clore, G. M., DeLano, W. L., Gros, P., Grosse-Kunstleve, R. W., Jiang, J. S., Kuszewski, J., Nilges, M., Pannu, N. S., Read, R. J., Rice, L. M., Simonson, T. & Warren, G. L. (1998). *Acta Cryst.* D**54**, 905–921.
Chuang, S. E., Burland, V., Plunkett, G., Daniels, D. L. & Blattner, F. R. (1993). *Gene*, **134**, 1–6.
Cochran, W. & Howells, E. R. (1954). *Acta Cryst.* **7**, 412–415.
Esnouf, R. M. (1997). *J. Mol. Graph. Model.* **15**, 132–134.
Esnouf, R. M. (1999). *Acta Cryst.* D**55**, 938–940.
Glauser, S. & Rossmann, M. G. (1966). *Acta Cryst.* **21**, 175–177.
Gottesman, S., Roche, E., Zhou, Y. & Sauer, R. T. (1998). *Genes Dev.* **12**, 1338–1347.
Howells, E. R. & Perutz, M. F. (1954). *Proc. R. Soc. London Ser. A*, **225**, 308–314.
Kessel, M., Wu, W., Gottesman, S., Kocsis, E., Steven, A. C. & Maurizi, M. R. (1996). *FEBS Lett.* **398**, 274–278.
Kraulis, P. (1991). *J. Appl. Cryst.* **24**, 946–950.
Levchenko, I., Luo, L. & Baker, T. A. (1995). *Genes Dev.* **9**, 2399–2408.
Merritt, E. A. & Bacon, D. J. (1997). *Methods Enzymol.* **277**, 505–524.
Missiakas, D., Schwager, F., Betton, J. M., Georgopoulos, C. & Raina, S. (1996). *EMBO J.* **15**, 6899–6909.
Navaza, J. (1994). *Acta Cryst.* A**50**, 157–163.
Nicholls, A. & Honig, B. J. (1991). *J. Comput. Chem.* **12**, 435–445.
Otwinowski, Z. & Minor, W. (1997). *Methods Enzymol.* **276**, 307–326.
Pak, M., Hoskins, J. R., Singh, S. K., Maurizi, M. R. & Wickner, S. (1999). *J. Biol. Chem.* **274**, 19316–19322.
Rohrwild, M., Coux, O., Huang, H. C., Moerschell, R. P., Yoo, S. J., Seol, J. H., Chung, C. H. & Goldberg, A. L. (1996). *Proc. Natl Acad. Sci. USA*, **93**, 5808–5813.
Rohrwild, M., Pfeifer, G., Santarius, U., Muller, S. A., Huang, H. C., Engel, A., Baumeister, W. & Goldberg, A. L. (1997). *Nature Struct. Biol.* **4**, 133–139.
Schirmer, E. C., Glover, J. R., Singer, M. A. & Lindquist, S. (1996). *Trends Biochem. Sci.* **21**, 289–295.
Seong, I. S., Oh, J. Y., Lee, J. W., Tanaka, K. & Chung, C. H. (2000). *FEBS Lett.* **477**, 224–229.
Seong, I. S., Oh, J. Y., Yoo, S. J., Seol, J. H. & Chung, C. H. (1999). *FEBS Lett.* **456**, 211–214.

Song, H. K., Hartmann, C., Ramachandran, R., Bochtler, M., Behrendt, R., Moroder, L. & Huber, R. (2000). *Proc. Natl Acad. Sci. USA*, **97**, 14103–14108.
Sousa, M. C., Trame, C. B., Tsuruta, H., Wilbanks, S. M., Reddy, V. S. & McKay, D. B. (2000). *Cell*, **103**, 633–643.
Terwilliger, T. C. & Berendzen, J. (1999). *Acta Cryst.* D**55**, 849–861.
Wilson, A. J. C. (1949). *X-ray Optics. The Diffraction of X-rays by Finite and Imperfect Crystals.* London: Methuen & Co. Ltd.
Yeates, T. O. (1988). *Acta Cryst.* A**44**, 142–144.
Yoo, S. J., Seol, J. H., Shin, D. H., Rohrwild, M., Kang, M. S., Tanaka, K., Goldberg, A. L. & Chung, C. H. (1996). *J. Biol. Chem.* **271**, 14035–14040.